Ocean Modelling 148 (2020) 101587

Contents lists available at ScienceDirect

Ocean Modelling

journal homepage: www.elsevier.com/locate/ocemod

# A box model to represent estuarine dynamics in mesoscale resolution ocean models

Giorgia Verri [a,*], Nadia Pinardi [b], Frank Bryan [c], Yu-heng Tseng [c,d], Giovanni Coppini [a], Emanuela Clementi [a]

[a] Centro Euro-Mediterraneo sui Cambiamenti Climatici, CMCC, Lecce, Italy
[b] Department of Physics and Astronomy, University of Bologna, Bologna, Italy
[c] National Centre for Atmospheric Research, Boulder, USA
[d] Institute of Oceanography, Nation Taiwan University, Taipei, Taiwan[1]

ARTICLE INFO

*Keywords:*
Estuarine dynamics
River plume dynamics
River–ocean interface
Estuary box model
Eddy resolving ocean model

ABSTRACT

Representing the net freshwater flux at river mouths is challenging for global and regional scale ocean modelling. Although rivers are well known to affect both the coastal and basin-wide circulation and dynamics, coarse resolution ocean models cannot resolve the estuarine dynamics and are usually forced at river outlets in a simplistic way, with climatological runoff and zero or constant salinity values. The aim of this study is to provide a more realistic representation of the estuarine water inputs to a coarse but eddy-resolving regional model.

First, the river volume transport and salinity values at the outlets are modelled with three different Estuary Box Models (EBMs) for stratified estuaries: the Knudsen relations model, a published EBM, called UCONN-NCAR EBM, which parameterizes the tidal inflow and mixing inside the estuary, and a new model, called CMCC-EBM. The CMCC EBM has been conceived to represent the estuarine processes coupled to a mesoscale resolving hydrodynamic model that resolves the entering flow field at the estuary mouth and it offers a new representation of the tidal inflow and a new salinity tidal mixing parameterization via horizontal diffusive processes.

The Ofanto and Po rivers flowing into the Adriatic Sea (northern part of the central Mediterranean Sea) are selected as case studies. The coupling of the eddy resolving ocean model to the CMCC EBM is found to outperform the one with the UCONN-NCAR EBM in the region of freshwater influence on the shelf areas.

## 1. Introduction

Over the past decades several theoretical as well as modeling studies (e.g. Chapman and Beardsley, 1989; Simpson et al., 1993; Kourafalou et al., 1996; Yankovsky and Chapman, 1997; Kourafalou, 1999; Garvine, 1999; Schiller and Kourafalou, 2010; MacCready and Geyer, 2010; among the others) have highlighted that the freshwater discharge dominates the dynamics of the shelf areas adjacent to estuaries, known as Regions of Freshwater Influence (ROFIs), by producing a "buoyant river plume", which consists of an offshore bulge and a coastal alongshore current due to the geostrophic adjustment.

More recent studies (e.g. Garvine and Whitney, 2006; Hordoir et al., 2008; MacCready et al., 2009; MacCready and Geyer, 2010 among others) have examined the role played by the ocean salty waters intruding into the estuaries, demonstrating that this intrusion drives the estuarine water exchange thus affecting the net estuarine outflow and salinity values. The connection of the estuary stratification with the coastal dynamics has been investigated and the forcings that determine the shape and intensity of the buoyant plume have been identified. The plume dynamics were found to be strongly tidal in the "near-field plume" (Jirka et al., 1981), which is the area immediately outside of the river mouth corresponding to the excursion length of the ebb tides. Winds also affect the river plume: downwelling winds facilitate the homogenization of the water column and tend to turn the plume into an along-shore current, while upwelling winds promote the water stratification and offshore drift (Chao, 1987). The role of wind stress is demonstrated to prevail over tides as the buoyant river inflow moves far from the outlet in the so named "far field plume" (MacCready et al., 2009).

Previous studies have focused on the effects of the freshwater discharge on the shelf and coastal circulation and dynamics, while fewer show their basin-wide effects. Among them, Rahmstorf (1995) speculated that an increasing freshwater inflow in the northern Atlantic is potentially able to reduce or even shut down the local overturning

* Corresponding author.
*E-mail address:* giorgia.verri@cmcc.it (G. Verri).
[1] Now at.

https://doi.org/10.1016/j.ocemod.2020.101587
Received 24 February 2019; Received in revised form 8 December 2019; Accepted 5 February 2020
Available online xxxx
1463-5003/

circulation. Skliris et al. (2007) demonstrated that the salinity increase observed in the Western Mediterranean dense water during 1965–2005 can be explained by about 50% from the salinity increase of the Levantine Intermediate Water due to damming of Black Sea and the Nile river. The remaining part is explained locally, and due to the reduction of the Ebro River runoff. Coles et al. (2013) showed that the Amazon River release has pathways into the western tropical and subtropical gyres of the North Atlantic. Verri et al. (2018) showed that river runoff affects the strength of the overturning circulation of the Central Mediterranean Sea, enhancing the amplitude of the secondary estuarine cells and reducing the intensity of the dominant anti-estuarine cell. Rivers are also demonstrated to reduce the volume of Adriatic dense water in the Southern Adriatic Sea of about 20% as a result of increased water stratification. Moreover, Tseng et al. (2016) and Sun et al. (2019) showed the impacts of different choices of freshwater inputs in an earth system climate model, concluding that river salinity effects are important at basin scale.

The above-mentioned studies indicate that global and regional ocean models require a good representation of the net freshwater release at river outlets. Global and regional ocean models cannot resolve the estuarine dynamics, due to low resolutions that cannot reach the spatial scales of the estuarine geometry and processes. Recently the University of Connecticut (UCONN) and the National Center for Atmospheric Research (NCAR) have jointly developed a reduced order Estuary Box Model (EBM) which interfaces the upstream river runoff with the ocean through a two-layer box model which represents the estuarine dynamics (Sun et al., 2017).

In this paper we compare the UCONN-NCAR EBM to a new estuary box model, the so-called CMCC EBM we developed at CMCC Foundation (Euro-Mediterranean Center on Climate Change), to be coupled explicitly with an eddy resolving mesoscale ocean general circulation model as described below.

The latter offers a new representation of the volume and salt conservation equations for three main reasons: (1) the CMCC EBM is conceived for coupling with regional eddy-resolving models which are expected to represent the advective dynamics near the river mouths better than low resolution, $O$(10–100 km), climate models which have been used with the UCONN-NCAR EBM; (2) the mixing due to tidal processes is parameterized by a turbulent salt diffusion parameter; (3) the tidal pumping enters both the volume and salt conservation equations through the flood tide inflow and the ebb tide outflow. The latter is embedded in the unknown estuarine outflow.

To show the impact of the EBM volume flux and salinity values on the quality of an ocean simulation, we applied the results of the EBMs to a regional ocean model in the central Mediterranean Sea and in particular to two estuaries in this area. The first is the highly-stratified estuary of the Ofanto river, which flows through Apulia in southern Italy and ends in the Southern Adriatic Sea. The second is the partially mixed delta of the Po river, one of the main rivers in Europe which discharges into the northern Adriatic Sea. For the Ofanto test case we compare an explicitly resolved estuary with the results of the two EBMs. For the Po test case we compare with open and free access observations of opportunity. This comparison is capable to differentiate among the two EBMs and the climatological fixed salinity approach with respect to simulating the river discharge and its associated salinity.

The final aim was to show that EBM inputs can in fact improve the shelf salinity in the vicinity of estuaries with respect to climatological, fixed salinity simulations.

The paper is organized as follows. Section 2 describes the three estuarine models. The method used to couple them to the regional ocean model is introduced in Section 3. Section 4 presents the selected case studies. The results of both the estuarine dynamics and the coastal dynamics are discussed in Sections 5 and 6. The summary and the conclusions are presented in Section 7.

## 2. The estuary box modelling

The presented study is placed in the framework of developing a conceptual and numerical modelling approach to simulate the effects of rivers on the coastal circulation in eddy-resolving general circulation models. The km-scale models cannot explicitly resolve the estuary dynamics; thus the idea of an "estuary box model" which transforms freshwaters and river discharges into estuary mouth volume and salinity fluxes was developed by Sun et al. (2017). The concept is as follows: at the river mouth, stratification can be relevant and the discharge is different from the river runoff far upstream, where the dynamics are driven by precipitation, hydrology and river geometry. The stratification and transport field at the estuary mouth can be approximated by two layer flow in several cases, where the lower layer enters the estuary and the upper layer discharges into the coastal area. The EBM gives the values of water volume flux and salinity at the river mouth, which in turn affects the coastal ocean dynamics. The precise analytical and numerical formulation of the boundary conditions in the ocean general circulation model are given in Section 3.

Three approaches for representing the estuary dynamics are considered: the simplest model is based on Knudsen's relation (Knudsen, 1900), the second on the UCONN-NCAR EBM (Sun et al., 2017) and the last on a new box model developed at CMCC and presented in this paper, the CMCC-EBM.

All the EBMs assume that the estuary region is a two-layer rectangular box with constant width $L_y$, depth $H$ and length $L_x$, as shown in Fig. 1. The estuary head is considered as the last section along the river network moving in the downstream direction where the salinity is still equal to zero and the estuary length, $L_x$ is set as the distance between the estuary head and the mouth. The estuary width, $L_y$ is the approximate estuary width or the width of the delta area, if several mouths are present for the same upstream conditions. The estuary depth, $H$, is chosen as a compromise between the river depth and the near mouth shelf bathymetry. The cross sections at the estuary mouth and the estuary head are open.

All the models are laterally and along channel averaged, steady-state and tidally averaged. The tidal cycle, i.e. the lunar day, includes both the flood tide and the ebb tide phases. It is about 50 min longer than the solar day thus we approximate with the solar day in this study.

The average over the tidal cycle is fully consistent with the estuaries classified as 'highly stratified' or 'partially mixed' (Fischer et al., 1979). In fact, these estuaries maintain the stratification over the tidal cycle. They may become unstable and mix only during the late ebb-tide phase (Geyer and Smith, 1987). A different treatment will be required in the future to consider 'well mixed' estuaries which might produce a destratified water column over the tidal cycle (MacCready and Geyer, 2010). The heat flux, precipitation and wind stress are not considered at this stage, although we know that their effects are relevant for some rivers (Chen and Sanford, 2009; Scully et al., 2005; Schroeder and Wiseman Jr., 1986). Furthermore, in this work we do not consider temperature effects because the estuary dynamics is, to the first order, dominated by salinity exchanges.

*The Knudsen's model.* The Knudsen's relation consists of two conservation equations for the volume and salt fluxes under the assumptions of (i) a rigid lid, and (ii) incompressible fluid. The model sketch is drawn in the top panel of Fig. 1. We hereafter refer to this model as Knudsen EBM.

The Knudsen's relation considers the following physical processes: the riverine water inflow at the estuary head, the ocean water inflow through the lower layer at the estuary mouth and the estuarine water outflow through the upper layer. The tidal effects and mixing processes are ignored in the equations, the upper layer salinity is generated instantaneously by unresolved processes in order to balance the salt inflow in the lower layer.

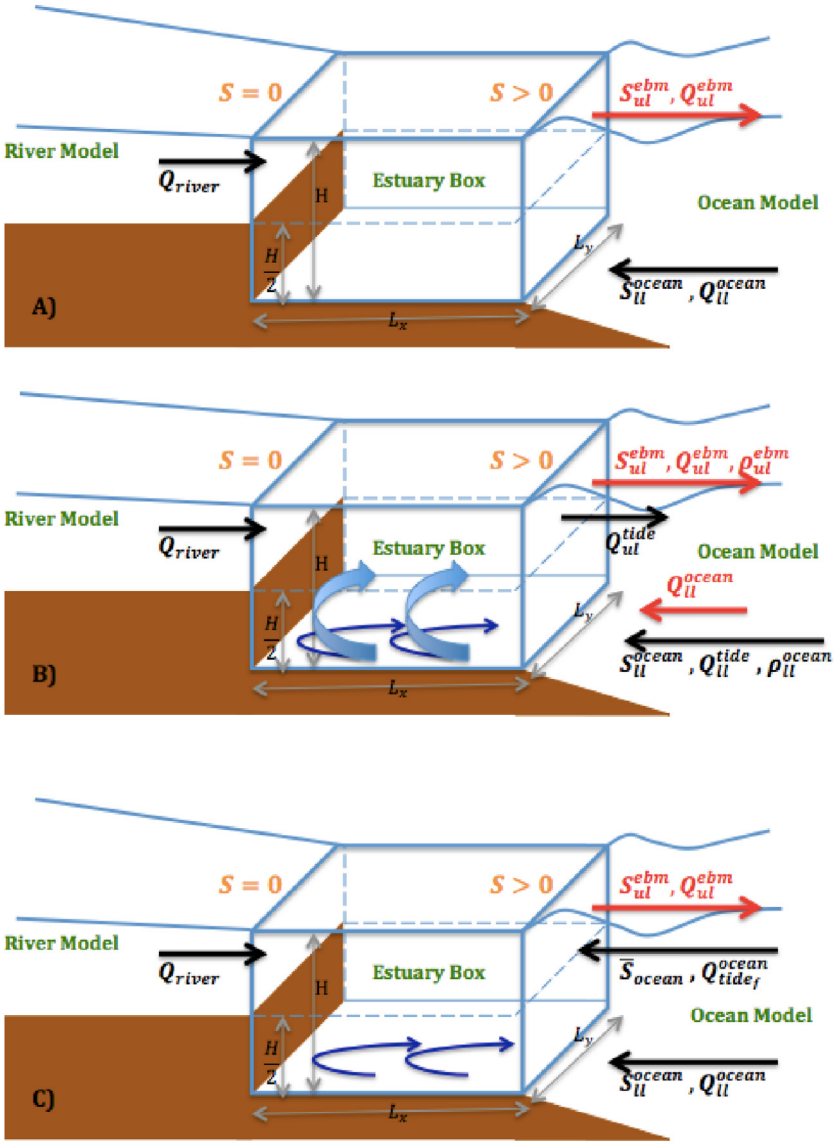


**Fig. 1.** Sketch of the three Estuary Box Models (EBMs) used in the paper: Knudsen relations model (top panel A), UCONN-NCAR EBM (middle panel B) and CMCC EBM (bottom panel C). The volume fluxes entering or exiting the box along with their salinities and densities are represented by arrows. Black arrows stand for input values from the ocean and river models, red arrows for the unknowns solved by the EBM. The pairs of blue arrows represent the tidal mixing, pairs of upward light-blue arrows stand for the shear mixing at the layer interface.

The conservation equations for the volume flux ($m^3/s$) and the salinity, averaged over the box and in time, are as follows:

$$Q_{ul}^{ebm} = Q_{river} + Q_{ll}^{ocean} \tag{1}$$

$$S_{ul}^{ebm} Q_{ul}^{ebm} = S_{ll}^{ocean} Q_{ll}^{ocean} \tag{2}$$

Quantities in (1) and (2) are distinguished between inputs and unknowns. The subscripts "ll" and "ul" stand for "lower layer" and "upper layer" respectively. The volume flux and salinity of the outflowing estuarine water, $Q_{ul}^{ebm}$ and $S_{ul}^{ebm}$, are considered as unknowns, while the $Q_{river}$, the volume flux of the river inflow at the estuary head, $Q_{ll}^{ocean}$ and $S_{ll}^{ocean}$, the volume flux and salinity of the ocean water inflow through the lower layer at the estuary mouth, are inputs.

Eq. (1) is obtained starting from the continuity equation with a rigid lid assumption and Eq. (2) is derived from the salinity equation under steady state conditions without considering diffusion.

*The UCONN-NCAR EBM.* The 2-layer steady state UCONN-NCAR EBM (Sun et al., 2017) is based on the concept of the potential energy anomaly proposed by Garvine and Whitney (2006). The model assumptions are (i) no surface layer forcing, (ii) incompressibility and (iii) hydrostatic balance. A sketch of the model is shown in the middle panel of Fig. 1.

The physical processes described are the riverine water inflow at the estuary head, the ocean water inflow through the lower layer at the estuary mouth, the estuarine water outflow through the upper layer at the mouth, the tidal pumping over a whole tidal cycle including the flood and the ebb tide, the tidal mixing at the bottom and the shear mixing at the layer interface.

The model consists of four equations: the continuity equation for the volume flux, the salinity equation which includes a parametrization of the tidal pumping, a Potential Energy (PE) equation, and a linear equation of state for seawater. The equations, averaged over the tidal cycle, are:

$$Q_{ul}^{ebm} = Q_{river} + Q_{ll}^{ocean} \tag{3}$$

$$\rho_{ul}^{ebm} Q_{ul}^{ebm} = \rho_{ll}^{ocean} Q_{ll}^{ocean} + \rho_0 Q_{river} + (\rho_{ll}^{ocean} - \rho_{ul}^{ebm}) m_{tides} Q_{ul}^{tides}/2 \tag{4}$$

$$PEF_{ul} = PEF_{river} + PEF_{ll} + PEF_{tp} + PEF_{tm} + PEF_{sm} \tag{5}$$

$$\rho = \rho_0 (1 + k_s S) \tag{6}$$

The subscripts "$tp$" and "$tm$" represent tidal pumping and tidal mixing respectively. The subscript "$sm$" represents the shear mixing term. $Q_{ul}^{tides}$ is the tidal volume flux that exits the upper layer during the ebb tide, $m_{tides}$ is the ratio between the areas of advected volumes during ebb or flood tide, $k_s = 7.7 * 10^{-4}$ psu$^{-1}$ is the haline contraction coefficient (Garvine, 1999) and $\rho_0 = 1000$ kg m$^{-3}$ is the freshwater reference density. Using Eq. (6) the upper and lower layer densities are defined: $\rho_{ul}^{ebm} = \rho_0(1 + k_s S_{ul}^{ebm})$ and $\rho_{ll}^{ocean} = \rho_0(1 + k_s S_{ll}^{ocean})$.

The UCONN-NCAR EBM formula for the average tidal volume flux during half a tidal cycle reads: $|Q_{ul}^{tide}| = Q_{tide_f}^{ocean} = 2\frac{u_{tide}}{\pi} L_y \frac{H}{2}$ with $u_{tide} = A\sqrt{g/H}$, where $A$ is the tidal amplitude.

The Potential Energy Flux terms, PEF (units of J/s), are detailed in Sun et al. (2017) and are not reproduced here.

The outflowing volume flux through the upper layer $Q_{ul}^{ebm}$, the salinity of outflowing water $S_{ul}^{ebm}$ and the volume flux of the ocean water entering the lower layer $Q_{ll}^{ocean}$ are the unknowns for this model, while the river volume flux at the estuary head, $Q_{river}$ and the salinity of inflowing ocean water through the lower layer, $S_{ll}^{ocean}$ are provided as inputs.

The tidal pumping effects are inserted in the last term of the RHS of Eq. (4) and the third term of the RHS of Eq. (5). The tidal mixing is included in the fourth term of the RHS of Eq. (5) and the shear mixing is represented in the last term of the RHS of Eq. (5). The detailed explanation of each of them can be found in Sun et al. (2017). Here it is only important to recall that the flood tide is considered to enter the estuary through both layers, while the ebb tide outflow involves the upper layer only (Simpson et al., 1990). Moreover the volume fluxes at the mouth during flood and ebb tides are also simplified as in Stommel and Farmer (1995). This means that there is no net volume flux due to tides in the continuity equation, while ebb and flood tides have a specific effect in the salinity and PE equations because of the density differences between waters removed and introduced at ebb and flood times. The assumption of a net tidal volume flux equal to zero is not necessarily true. Moreover, the empirical formula used to represent the flood tide inflow and the ebb tide outflow generalize the ones proposed by Stommel and Farmer (1995): the flood tide inflow can vary from a semi-ellipse to a semi-circle form, while the ebb tide outflow has a rectangular jet-like form. The coefficient $m_{tides}$ in Eq. (4) comes out from this geometrical simplification and require a quite complex calibration. These assumptions on the tidal pumping limit the performance of the model when applied to poorly monitored estuaries. In addition present day tidal models, such as the Oregon State University Tidal Prediction Software (OTPS, Egbert and Erofeeva, 2002) used in this study to force the CMCC EBM, resolve the tidal coastal dynamics up to few km. A new representation of the flood tide inflow and the ebb tide outflow without any parameterization is then introduced in the CMCC-EBM, as described in the following section.

*The CMCC EBM.* A new EBM is developed in this paper, from the basic assumption that the lower layer salinity and volume inflow are specified by the eddy resolving ocean model near the coasts. The barotropic volume inflow due to tides comes from the OTPS (Egbert and Erofeeva, 2002) barotropic model because the eddy resolving ocean model used here does not include tides. The basic equations used are the continuity equation within the incompressible assumption and the salinity conservation equation as in the case of the UCONN-NCAR EBM. However, we do not need a third equation for the potential energy as in the UCONN-NCAR EBM because we have a total of two unknowns, the upper layer volume flux and the upper layer salinity. Furthermore, we add the tidal inflow in the continuity equation and in the salinity conservation equation and we parameterize the tidal mixing in the salinity equation in a different way of UCONN-NCAR EBM. The model sketch is drawn in the bottom panel of Fig. 1.

The tidally averaged equations are as follows:

$$Q_{ul}^{ebm} = Q_{river} + Q_{ll}^{ocean} + H L_y u_{tide_f} \tag{7}$$

$$S_{ul}^{ebm} Q_{ul}^{ebm} = S_{ll}^{ocean} Q_{ll}^{ocean} + \overline{S}_{ocean} H L_y u_{tide_f} + K_{S_H} H L_y \frac{\overline{S}_{ocean}}{L_x} \tag{8}$$

The inputs are the volume flux $Q_{ll}^{ocean}$ and salinity $S_{ll}^{ocean}$, the depth averaged ocean salinity $\overline{S}_{ocean}$ at the estuary mouth, the tidal velocity normal to the estuary mouth $u_{tide_f}$ and the river volume flux $Q_{river}$ at the estuary head. The volume flux $Q_{ul}^{ebm}$ and salinity $S_{ul}^{ebm}$ of the outflowing estuarine water through the upper layer are the model unknowns.

We describe the ocean water inflow as a baroclinic bottom inflow (second term on the RHS of Eq. (7) and first term on the RHS of Eq. (8)) and a barotropic tidal inflow during the flood tide phase (third term on the RHS of Eq. (7) and second term on the RHS of Eq. (8)). We describe the tidal mixing by considering that the horizontal diffusion of salt along the estuary (last terms on the RHS of Eq. (8)) is driven by the tides. We represent the river inflow at the estuary head as a volume flux (first term on the RHS of Eq. (7)) with zero salinity.

Appendix A provides a comprehensive demonstration of the governing equations of the CMCC EBM.

Unlike in the UCONN-NCAR EBM, the $Q_{ll}^{ocean} = \frac{H}{2} L_y u_{ll}^{ocean}$ is treated as an input variable calculated from the daily ocean velocity provided by the eddy resolving ocean model, $u_{ll}^{ocean}$, considered to be positive if it is landward oriented, and equal to zero if seaward oriented. Thus, $u_{ll}^{ocean}$ is the averaged horizontal velocity component in a box next to the river mouth as detailed in Section 4.

With regard to the tidal pumping, we follow the theoretical approach proposed by Simpson et al. (1990) with a barotropic tidal inflow during the flood tide $Q_{tide_f}^{ocean} = H L_y u_{tide_f}$ and a stratified outflow (through the upper layer) during the ebb tide, as done in the UCONN-NCAR EBM. However we do not assume that the tidal pumping inflow/outflow has the same amplitude, thus there is a tidal pumping term in the continuity equation.

We also physically solve the tidal pumping with no empirical formula (the full derivation is shown in Appendix A) and we provide the barotropic velocity corresponding to the flood tide, $u_{tide_f}$, while the outgoing tidal velocity during the ebb tide is embedded in the unknown estuarine water outflow $Q_{ul}^{ebm}$. The $u_{tide_f}$ is computed from the hourly outputs of the OTPS (Egbert and Erofeeva, 2002), considered as flood tide values if landward oriented and averaged daily. The flood tide volume flux is thus given by $Q_{tide_f}^{ocean} = H L_y u_{tide_f}$. The horizontal mixing coefficient for salt is computed following Banas et al. (2004): $K_{S_H} = 0.035\, L_y\, u_{tide_f}$.

It is worth to point out again that the CMCC EBM receives as input the lower layer transport from the mesoscale resolving general circulation model. Thus, it does not need a third conservation equation to solve for the lower layer volume inflow. In CMCC EBM only four parameters (the geometry coefficients $L_y$, $L_x$, $H$ and the turbulent diffusion coefficient $K_{S_H}$) need to be calibrated.

## 3. Coupling the estuary box model with an eddy resolving regional ocean model

Fig. 2 shows the computational domain of the regional ocean model (Verri et al., 2018) used in this study, based on the three-dimensional finite difference code NEMO v3.4 (Madec, 2008). The model grid covers the central Mediterranean Sea with a horizontal resolution of about 2.2 km (2.5 km in the meridional direction and 1.7–2.2 km in the zonal direction). The vertical discretization consists of 121 unevenly spaced z-levels with increased resolution at the top and the bottom and partial cells at the bottom.

The eddy-resolving regional model is one-way nested in a 1/16° resolution, 72 levels, numerical ocean analysis and forecasting model of the Mediterranean Sea (Oddo et al., 2009). The robustness of this model has been demonstrated in Verri et al. (2018) who provide an interannual comparison with in situ and satellite observations in the open sea. Verri et al. (2018) follow Oddo et al. (2005) approach where

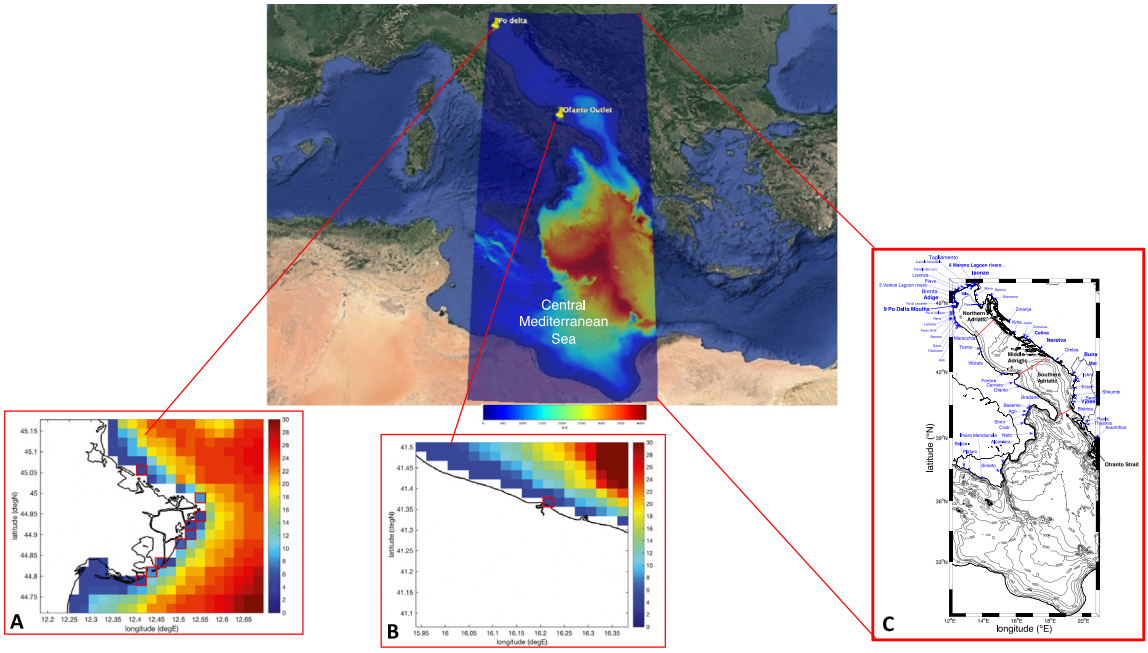


**Fig. 2.** Top panel: The regional model computational domain. Shaded colours show the bathymetry. Panel A: Zoom on Po ROFI bathymetry. Edged red cells are the Po river mouths. Panel B: Zoom on Ofanto ROFI bathymetry. Edged red cell is the Ofanto mouth. Panel C: The regional ocean model domain with: black isolines showing the bathymetry values, red lines defining the Adriatic sub-regions and the Ionian Sea, blue stars and arrows indicating the represented river mouths. Panel C picture is from Verri et al. (2018).

the runoff salinity is taken to have ad hoc values, based upon heuristic reasoning. In this paper we remove the ad hoc assumptions about the salinity at the river mouth.

As the rivers are not explicitly represented as lateral open boundary conditions, due to the coarse resolution of the eddy resolving regional ocean model, the riverine inputs of volume and salinity are treated as boundary conditions for the vertical velocity and the vertical diffusive salinity flux at the sea surface (Beron-Vera et al., 1999; Tseng et al., 2016). A detailed explanation of the formulation used by NEMO for the riverine release as surface boundary conditions is provided in Appendix B.

Given the upper layer volume outflow, $Q_{ul}^{ebm}$, and the upper layer salinity $S_{ul}^{ebm}$, both computed by the EBMs, the surface boundary conditions for the vertical velocity and the diffusive salt flux are written as:

$$w\Big|_{z=\eta} = \frac{\partial \eta}{\partial t} + \vec{u}_h\Big|_{z=\eta} \cdot \nabla_h \eta + (E - P - Q_{ul}^{ebm}/A) \tag{9}$$

$$k_v \frac{\partial S}{\partial z}\Big|_{z=\eta} = (E - P)S(\eta) + \frac{Q_{ul}^{ebm}}{A} S_{ul}^{ebm} \tag{10}$$

where $w\Big|_{z=\eta}$ is the vertical velocity at the sea surface, $\eta$ is the sea surface elevation, $\vec{u}_h$ is the horizontal velocity at the sea surface, $E$ is the evaporation rate (units of m/s), $P$ is the precipitation rate (units of m/s), $A$ is the horizontal area of the sea grid cell corresponding to the river mouth, and $k_v$ is the vertical diffusivity coefficient. The $S_{ul}^{ebm}$ and the $Q_{ul}^{ebm}$ are prescribed at river mouth grid points which approximate the river mouth positions.

## 4. Case studies

*The Ofanto river highly stratified estuary.* We chose the funnel-shaped estuary of the Ofanto river as our first case study. This "semi-perennial" river flows through Southern Italy and ends in the Southern Adriatic Sea (Fig. 2 and top panel Fig. 3). The mean annual runoff is 14.92 $m^3\ s^{-1}$ (Raicich, 1996) and the mean annual tidal amplitude recorded at the tidal gauge closest to the river mouth is 0.04 m (Guarnieri et al., 2013).

We performed several experiments using the three EBMs with river runoff, $Q_{river}$, from a simulation performed with the WRF-Hydro model (Verri et al., 2017), as no observations were available at the estuary head. The period of interest chosen was January–March 2011, which was characterized by a high river discharge and two flooding events (bottom panel of Fig. 3).

In order to characterize the stratification of the Ofanto river, we estimated the "flow ratio" parameter $F$ (Fischer et al., 1979) for the period of simulation:

$$F = \overline{u_{tidef}}/\overline{u}_{river} = 0.02 \tag{11}$$

where $\overline{u_{tidef}}$ is the averaged flood tide velocity computed by the OTPS system and $\overline{u}_{river}$ is the mean river streamflow modelled at the estuary head. Values of $F$ less than 0.1 are classified as highly stratified, thus the Ofanto estuary is a "sharply stratified" estuary.

The geometrical parameters of the Ofanto estuary are: the estuary width, $L_y = 25$ m; the estuary depth, $H = 5$ m; and the estuary length, $L_x = 1$ km which are kept equal for all the three EBMs. The estuary length $L_x$ complies with the results of a monitoring campaign that estimated the length of the salt intrusion to be about 1 km upstream of the Ofanto mouth (personal communication of the Water Research Institute of the National Research Council, CNR-IRSA). The UCONN-NCAR EBM requires additional parameters. We extracted the tidal period, $T$, and the tidal amplitude, $a_{tide}$, from Guarnieri et al. (2013), while the bottom drag coefficient $C_d$, the tidal mixing efficiency $\epsilon$, the shear mixing efficiency $\gamma$ and the entrainment constant at the layer interface $\alpha$ are the values used in the literature (Sun et al., 2017).

The salt and volume of the inflowing ocean water, i.e. $S_{ll}^{ocean}$ and $Q_{ll}^{ocean}$, are computed as volume weighted averages of the ocean model grid points, three by three grid points in the horizontal and three vertical grid levels from the bottom, surrounding the approximate position of the Ofanto river mouth. In detail, the mesoscale general circulation model considers a minimum depth at the coasts of 5 meters and it considers six levels for this depth. The lowest three model levels are inside the lower layer of the EBM model, i.e. from 2.5 m to 5 m depth.

Two additional fields are required by the CMCC EBM, i.e. the flood tide velocity $u_{tidef}$ and the depth averaged ocean salinity $\overline{S}_{ocean}$. The

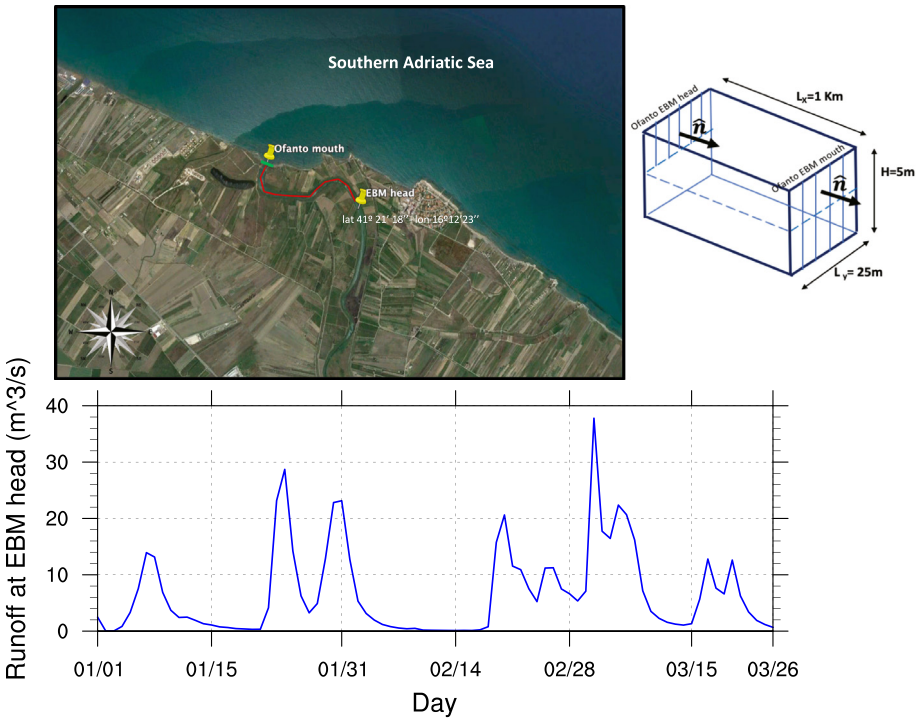


**Fig. 3.** The Ofanto river case study. Top-left panel: the map of the river outlet and estuary geometry (Google Earth image). The green line is the box width, $L_y$. The red line estimates the estuary length, $L_x$. Top-right panel: Sketch of the Ofanto estuary Box. Bottom panel: time series of the runoff at the estuary head as simulated by WRF-Hydro model during January–March 2011.

former is provided by the OTPS system, as described in Section 2; the latter is a spatially weighted average covering all the vertical levels in a three by three grid point area. An overview of the EBMs settings for the Ofanto estuary case is provided in Table 1.

*The Po river partially mixed delta.* The second case study is the delta-shaped estuary of the Po river. This is the main freshwater source of the central Mediterranean Sea and the second in the whole Mediterranean basin. The mean annual runoff is 1492 $m^3\ s^{-1}$ (Ludwig et al., 2009) and the mean annual tidal amplitude recorded at the tidal gauge closest to the river mouth is 0.09 m (Guarnieri et al., 2013). Near the mouth, the river network creates a wide delta with hundreds of small channels and nine main branches. The map of the river delta is given in Fig. 4.

A set of experiments to represent both the estuarine dynamics and the ROFI dynamics of the Po river were performed from January to June 2009. This period was chosen according to the observation availability close to the river mouths. The estuary head runoff, $Q_{river}$, is provided by the observations at the Pontelagoscuro station. This time range includes a major flood event on May 2nd with a recorded runoff exceeding 8000 $m^3/s$ (Fig. 4).

Fischer's "flow ratio" (11) for the Po river is 0.43. This means that the Po estuary is a "partially mixed" estuary: the tidal flow is comparable with the river flow and the induced vertical mixing smooths the salinity gradient, although the stratification of the exchange flow persists over a whole tidal cycle. The representation of the estuarine dynamics as a two-layer exchange flow is therefore still reasonable.

We considered the inflowing tidal velocity at the river mouth, $\overline{u_{tide_f}}$, as given by OTPS and the river streamflow velocity at the estuary head, $\overline{u}_{river}$, as provided by Pontelagoscuro station.

Given the relatively coarse resolution of our ocean model, it is not really possible to distinguish $u_{ll}^{ocean}$ affecting one mouth with respect to the other. Thus we decided to take a box model for all the Po river mouths together. In the future, if the resolution of the regional model will increase $u_{ll}^{ocean}$ will be different at different Po river branches and different EBMs could be applied to each of them.

**Table 1**
EBMs settings for the Ofanto estuary and the Po delta cases.

| EBM | Ofanto estuary | Po delta |
|---|---|---|
| Knudsen EBM | | |
| Geometry coefficients $L_x$, $L_y$, $H$ (m) | 1000, 25, 5 | 20 000, 20 000, 5 |
| Runoff forcing $Q_{river}$ ($m^3\ s^{-1}$) | WRF-Hydro model | Pontelagoscuro station |
| Ocean forcings $S_{ll}^{ocean}$ (psu), $u_{ll}^{ocean}$ ($m\ s^{-1}$) | NEMO regional model | NEMO regional model |
| UCONN-NCAR EBM | | |
| Geometry coefficients $L_x$, $L_y$, $H$ (m) | 1000, 25, 5 | 20 000, 20 000, 5 |
| Tidal coefficients $T_{tide}$ (s), $A_{tide}$ (m) | 44 712, 0.04 | 44 712, 0.09 |
| Physical coefficients $\epsilon$, $\gamma$, $\alpha$ | 0.2, 0.002, 0.01 | 0.2, 0.002, 0.01 |
| Runoff forcing $Q_{river}$ ($m^3\ s^{-1}$) | WRF-Hydro model | Pontelagoscuro station |
| Ocean forcings $S_{ll}^{ocean}$ (psu) | NEMO regional model | NEMO regional model |
| CMCC EBM | | |
| Geometry coefficients $L_x$, $L_y$, $H$ (m) | 1000, 25, 5 | 20 000, 20 000, 5 |
| Physical coefficient $c_k = \frac{K_{S_H}}{L_y u_{tide_f}}$ | 0.035 | 0.035 |
| Runoff forcing $Q_{river}$ ($m^3\ s^{-1}$) | WRF-Hydro model | Pontelagoscuro station |
| Ocean forcings $S_{ll}^{ocean}$, $\overline{S}_{ocean}$ (psu), $u_{ll}^{ocean}$ ($m\ s^{-1}$) | NEMO regional model | NEMO regional model |
| Tidal forcing $u_{tide_f}$ ($m\ s^{-1}$) | OTPS model | OTPS model |

The simplified set-up of the Po delta consists of an estuary box with length $L_x = 20$ km, width $L_y = 20$ km, and depth $H = 5$ m. The

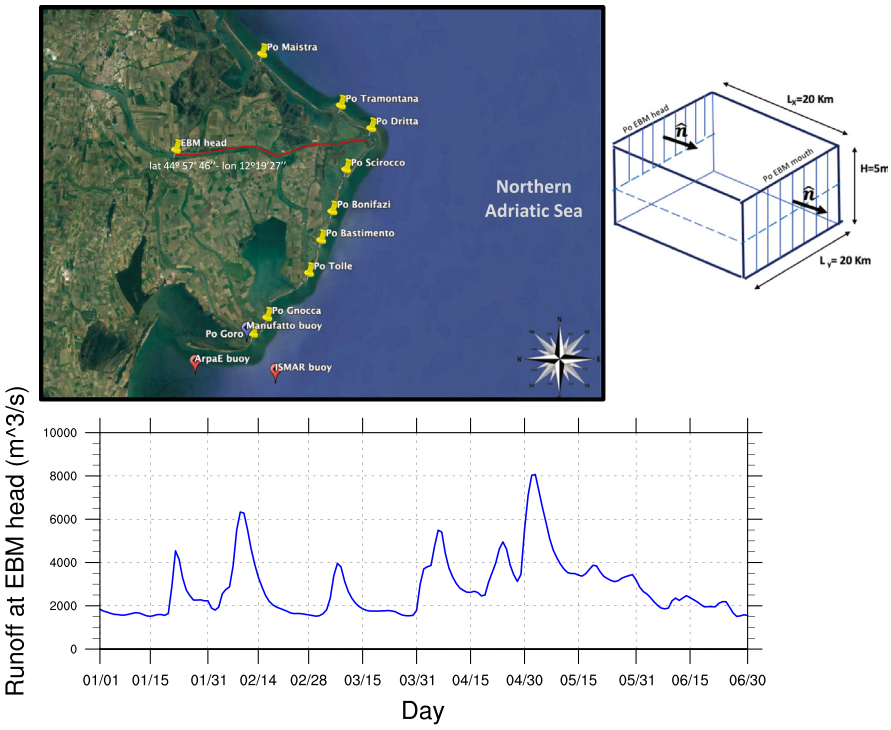


**Fig. 4.** The Po river case study. Top-left panel: the map of the delta geometry (Google Earth image) and the river mouths, i.e. Po di Maistra, Po della Pila (which splits into Po di Tramontana, Po di Dritta, Po di Scirocco, Po di Bonifazi and Po di Bastimento), Po di Tolle, Po di Gnocca, and Po di Goro (yellow markers). The combined width of all the Po mouths gives the box width, $L_y$. The red line estimates the estuary length, $L_x$. The red markers off are the ISMAR and ArpaE buoy positions. The blue marker is the Manufatto buoy position. Top-right panel: Sketch of the Po delta Box. Bottom panel: time series of the runoff at the head of the estuary as recorded by Pontelagoscuro gauge station during January–June 2009.

estuary length $L_x$ complies with the results of a monitoring campaign that estimated the length of the salt intrusion to be about 20 km upstream of Po di Dritta mouth, i.e. the easternmost mouth at the delta (personal communication of the Regional Agency for the Environmental protection, ArpaE). The estuary width $L_y$ is taken as a combined width of all of the Po mouths. The estuary depth $H$ is calculated as the bathymetry of the surrounding sea cells of our eddy resolving regional ocean model. Regarding the UCONN-NCAR EBM, the tidal coefficients (i.e. the tidal period, $T$, and the tidal amplitude $a_{tide}$) are based on observations following Guarnieri et al. (2013). The other coefficients follow the reference values given by Sun et al. (2017), as in the Ofanto river case.

The salt and volume flux of the inflowing ocean water, $S_{ll}^{ocean}$ and $Q_{ll}^{ocean}$, are computed as volume weighted averages for the lowest 3 vertical levels of the ocean model and a three by three grid point area around the mouth of Po di Dritta. The additional fields required by the CMCC EBM, i.e. the flood tide velocity $u_{tide\,f}$ and the depth averaged ocean salinity $\overline{S}_{ocean}$, are computed as with the Ofanto river. The upper layer volume flux from the EBM, $Q_{ul}^{ebm}$, is distributed among the delta mouths (following the percentages in Provini et al. (1992)) which correspond to different grid points in the ocean model. An overview of the EBMs settings for the Po delta case is provided in Table 1.

## 5. Salinity and volume flux estimates from the EBMs

In this section the experiments performed with the three EBMs are compared and evaluated for the Ofanto and Po river study cases. Table 2 summarizes the order of magnitude of the volume fluxes entering the estuary box. The CMCC EBM shows the largest ocean water intrusion for the Ofanto and Po rivers due to the calculation of $Q_{ll}^{ocean}$ from the ocean model velocities. For the $Q_{tide_f}^{ocean}$ differences are evident only for the Ofanto.

Fig. 5 shows the salinity (top panel) and volume flux (bottom panel) of the outflowing estuarine waters for the Ofanto. Similarly Fig. 6 refers

**Table 2**
Order of magnitude of the volume fluxes estimated for the three EBMs.

| | Volume fluxes ($m^3\ s^{-1}$) | Ofanto river | Po river |
|---|---|---|---|
| $Q_{river}$ | | 10 | $10^3$ |
| $Q_{ll}^{ocean}$ | CMCC-EBM | 1 | $10^3$ |
| | UCONN-EBM | $10^{-2}$ | 1 |
| | Explicit Estuary | 1 | |
| $Q_{tide_f}^{ocean}$ | CMCC-EBM | $10^{-1}$ | $10^3$ |
| | UCONN-EBM | 1 | $10^3$ |

to the Po. In all the panels of Figs. 5 and 6 the green line time-series show the salinity and the volume flux used in Verri et al. (2018) to force the eddy resolving regional ocean model at the river mouths. The water volume fluxes are monthly climatologies for the Ofanto river (Raicich, 1996) and daily means observed at Pontelagoscuro station for the Po river. The salinity values are taken to be constant, i.e. 15 psu for the Ofanto and 17 psu for the Po river. We call both the salinity and volume fluxes from Verri et al. (2018) climatological estimates.

The salinity computed by Knudsen's EBM (blue lines in the top panels of Figs. 5 and 6) often drops to zero over several days for both case studies. This is an unreasonable result and reveals the major weakness in Knudsen's model which does not include tidal effects: the outflowing water salinity is equal to the zero salinity values at the estuary head if there is no lower layer inflow of salty waters from the ocean.

For the Ofanto (Fig. 5), there are no significant differences between UCONN and CMCC EBMs in both discharge and outflowing salinity except for a few days. To note that the discharge time series of Knudsen and CMCC EBM are nearly overlapped as the tidal volume flux is not relevant for this case study. Moreover, the discharge time series of UCONN-NCAR EBM almost overlaps the inflowing volume flux at the estuary head (the orange line). This is due to the fact that the lower

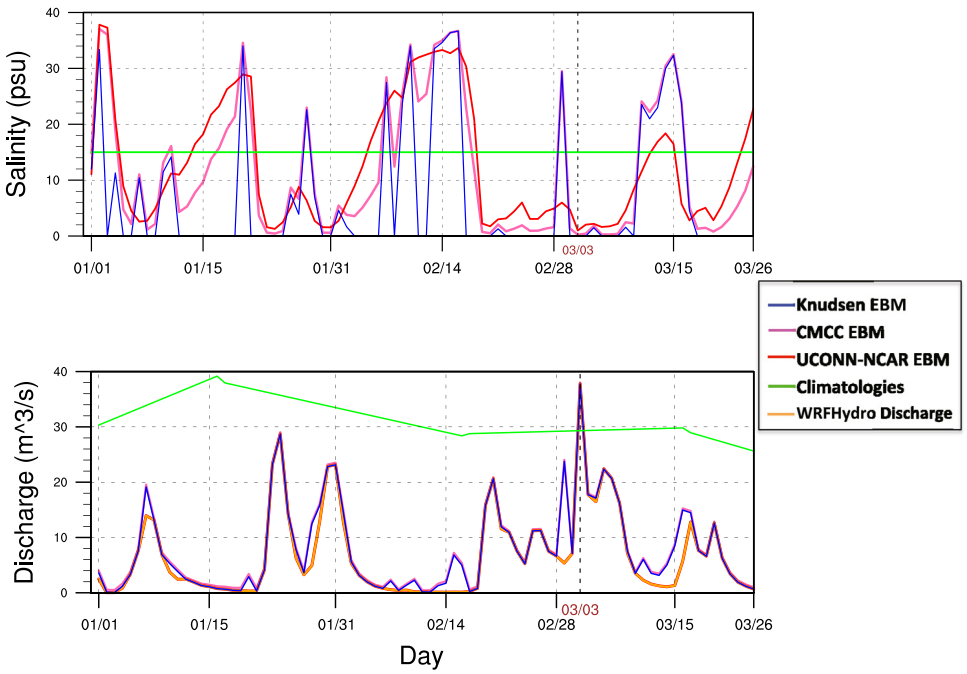


**Fig. 5.** Outflowing salinity $S_{ul}^{ebm}$ (upper panel) and volume flux $Q_{ul}^{ebm}$ (lower panel) of the Ofanto EBMs. The green lines are the climatological estimates following Verri et al. (2018). For completeness, the estuary head runoff by WRF-Hydro has been added in the lower panel. This overlaps the UCONN-NCAR EBM volume flux.

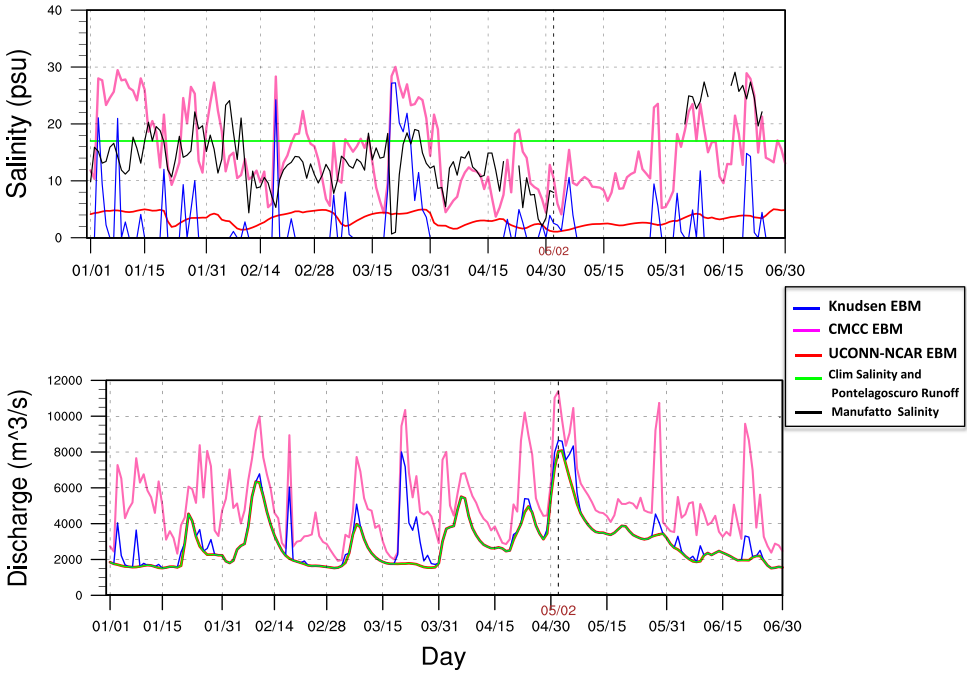


**Fig. 6.** Outflowing salinity $S_{ul}^{ebm}$ (upper panel) and volume flux $Q_{ul}^{ebm}$ (lower panel) of the Po EBMs. The green lines are the salinity climatological estimate and the observed volume flux following Verri et al. (2018). The black line in the upper panel refers to the Manufatto gauge station.

layer ocean volume inflow and the tidal volume flux are both found to be small in UCONN-NCAR EBM (see Table 2). On the other hand the UCONN-NCAR EBM shows a relevant role of the tidal pumping parameterization which ensures the outflowing salinity is not far from the CMCC EBM one despite the orders of magnitude difference in the ocean volume inflows.

For the Po (Fig. 6), UCONN-NCAR and CMCC EBMs radically differ in terms of both salinity and discharge: a higher salinity and volume flux of the outflowing estuarine water was simulated by the CMCC EBM. The CMCC EBM shows a stronger intrusion of the salty waters at the bottom of the estuary mouth as shown in Table 2. Moreover the two models solve the tidal pumping and the tidal mixing processes in different ways, which become particularly evident in the Po as this is a partially mixed estuary with strong tidal effects.

The additional comparison with the observed salinity (black time-series) in Fig. 6 shows that the CMCC EBM outperforms the other models. To note that the observations refer to a gauge station located close to the Po di Goro outlet (Fig. 4) but in a secondary channel.

Starting from the definition of the gradient Richardson number, $Ri = \frac{N^2}{(du/dz)^2} = \frac{g}{\rho_0}\frac{d\rho/dz}{(du/dz)^2}$, the time series of $Ri$ has been computed as

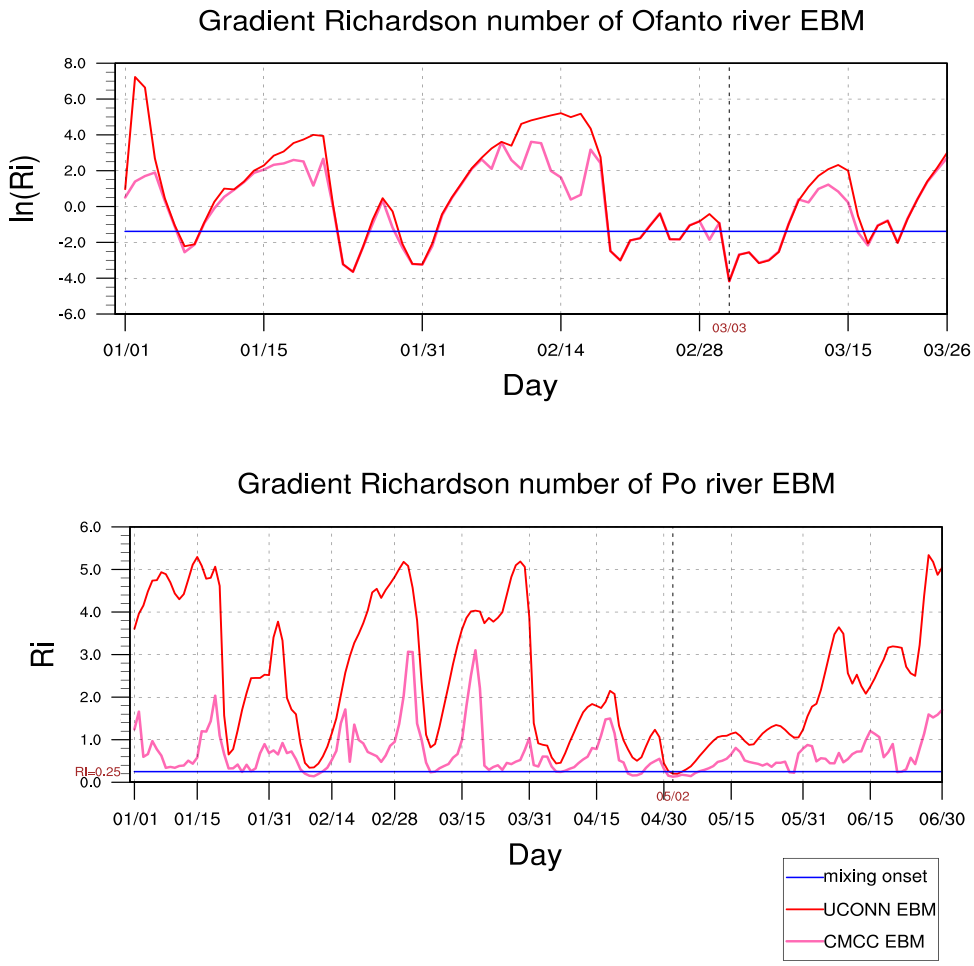


**Fig. 7.** Time series of the gradient Richardson number in the estuary box of the Ofanto river (upper panel) and the Po river (lower panel). The blue line, Ri = 0.25, is the well-known onset for mixing. The upper panel shows a semi-log plot because the Ofanto river is a highly-stratified estuary.

follows: $Ri_{ebm} = \frac{\frac{g}{\rho_0}\frac{d\rho}{dz}}{(\frac{du}{dz})^2} = \frac{g\frac{k_s}{\rho_0}\frac{S_{ll}^{ocean}-S_{ul}^{ebm}}{H/2}}{\left(\frac{u_{ll}^{ocean}+2u_{tide_f}-u_{ul}^{ebm}}{H/2}\right)^2}$ with the assumption that the density is a linear function of the salinity and $k_s = 7.7 * 10^{-4}$ psu$^{-1}$. The time series of $Ri_{ebm}$ in Fig. 7 shows that in both the Po and Ofanto, UCONN-NCAR EBM reaches higher values than CMCC EBM, thus suggesting that turbulent mixing across the stratification is weaker in UCONN-NCAR than in the CMCC EBM.

## 6. Effects of the different EBMs on the ROFI

The river volume fluxes and salinities computed by UCONN-NCAR and CMCC EBM were imposed in two simulations of our eddy resolving regional ocean model, one focused on the Ofanto ROFI area and the other in the Po ROFI. In both cases, the model covers the whole area depicted in Fig. 2, however the timing of the experiments is different as explained in the previous section.

For the Ofanto ROFI, four experiments were carried out: a "climatological" experiment based on the ocean model forced at river mouths by climatological runoff and a constant salinity of 15 psu. Two other experiments were performed by coupling the ocean model with the CMCC EBM and the UCONN-NCAR EBM volume and salinity fluxes (Fig. 5). A fourth experiment, referred to as the "explicit estuary", was performed with the eddy resolving regional ocean model by modifying the model coastline to include 10 km inlet simulating the Ofanto estuary. This "explicit estuary" experiment is forced at the inlet head with the runoff computed by the hydrological modelling system described by Verri et al. (2017) and with salinity equal to zero. This experiment is a coarse representation of the Ofanto estuary geometry and it allows for the salt intrusion to occur due to the physics of the eddy resolving model. It is indeed a coarsely resolved estuary (the horizontal model resolution is around 2 km) but it contains 6 vertical levels where the salt intrusion can develop. Thus, it is considered our control or most realistic scenario for the Ofanto estuary, to be used for comparison with the other three experiments because no observational data were available in the ROFI area.

Fig. 8 shows the daily sea surface salinity in the Ofanto ROFI during an upwelling wind regime for the western coast of the Adriatic basin, which promotes the development of the Ofanto plume. The coupled EBMs and ocean models, represent a well-defined river plume, are close to the benchmark experiment and outperform the climatological experiment, which is unable to reproduce the plume. Moreover, the estimate of the $Q_{ll}^{ocean}$ from the "explicit estuary" experiment has been computed (Table 2). It shows the same order of magnitude of the CMCC EBM one, not UCONN-NCAR.

For the Po ROFI, three experiments were carried out: a climatological experiment with the eddy resolving regional ocean model forced by the Pontelagoscuro runoff and a constant salinity of 17 psu, and two experiments with the ocean model forced by the outflowing salinity and volume outflow computed by the CMCC and UCONN-NCAR EBMs (Fig. 6). Fig. 9 shows the daily sea surface salinity during an upwelling wind event, which supports the offshore spreading of the Po plume. The experiments performed by coupling the EBMs with the eddy resolving regional ocean model represent a well-defined plume, while the climatological approach shows a much weaker development.

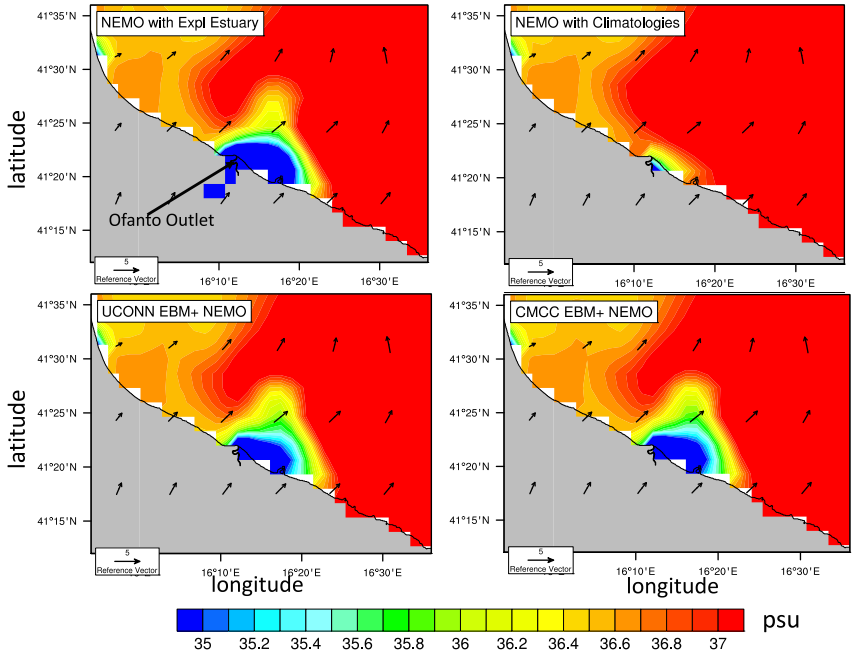


**Fig. 8.** Daily SSS (psu) of the Ofanto ROFI when upwelling wind regime (black arrows), i.e. on March 3rd 2011. TopLeft: Exp1, NEMO with explicit estuary set-up. TopRight: Exp2, NEMO with climatological river release. BottomLeft: Exp3, coupled UCONN-NCAR EBM + NEMO BottomRight: Exp4, coupled CMCC EBM + NEMO.

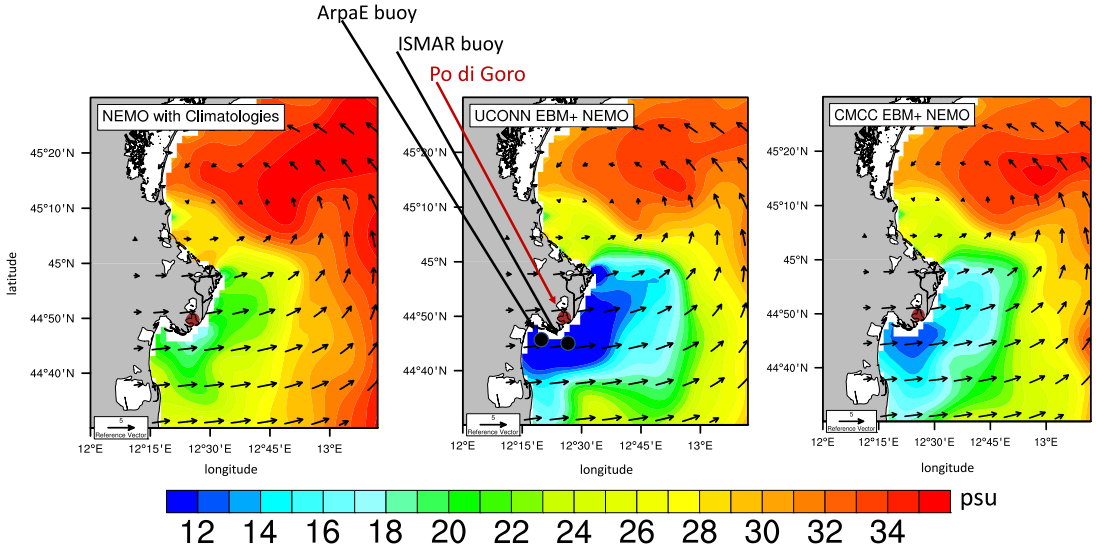


**Fig. 9.** Daily SSS (psu) of the Po ROFI when upwelling wind regime (black arrows), i.e. on May 20th 2009. Left: Exp1, NEMO with climatological river release. Middle: Exp2, coupled UCONN-NCAR EBM + NEMO. Right: Exp3, coupled CMCC EBM + NEMO. Dots and arrows indicate the locations of Po di Goro mouth and ISMAR and ARPAE buoys.

**Table 3**
Statistical indices for validation of the salinity by comparison with the ISMAR buoy. RMSE = root mean square error, CORR = time correlation.

| Statistics on salinity | RMSE | BIAS | CORR |
|---|---|---|---|
| CMCC EBM + NEMO | 4.05 | +0.25 | 0.61 |
| UCONN EBM + NEMO | 4.66 | +0.61 | 0.49 |
| NEMO with Climatologies | 5.06 | +3.53 | 0.55 |

**Table 4**
Statistical indices for validation of the salinity by comparison with the ARPAE buoy. RMSE = root mean square error, CORR = time correlation.

| Statistics on salinity | RMSE | BIAS | CORR |
|---|---|---|---|
| CMCC EBM + NEMO | 4.45 | +0.05 | 0.69 |
| UCONN EBM + NEMO | 5.48 | −2.06 | 0.67 |
| NEMO with Climatologies | 6.67 | +5.43 | 0.69 |

The validity of the model was evaluated by comparing the modelled salinity with the observed salinity at two buoys maintained by the Institute of Marine Sciences (ISMAR) and the Emilia Romagna Environmental Protection Agency (ArpaE). The ArpaE buoy is located 7 km offshore of the Po di Goro mouth at a 1 m depth. The ISMAR buoy (Ravaioli et al., 2016) is 5 km offshore at a 1.7 m depth. The buoys are indicated in the top panel of Fig. 4 and in the middle panel of Fig. 9. The time series in Figs. 10 and 11 show the comparisons. The coupled system with CMCC EBM was found to provide the lowest root mean square errors, as reported in Tables 3 and 4. Conversely, the climatological experiment gave the largest errors. At the ISMAR buoy, the salinity skill of UCONN-NCAR EBM was similar to CMCC-EBM, however for the ArpaE buoy the CMCC EBM was better

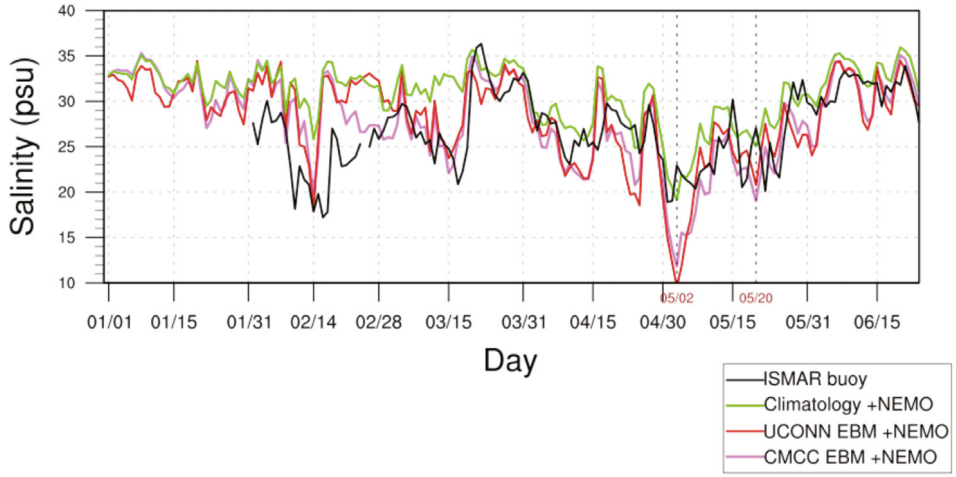


**Fig. 10.** Time series of observed and modelled salinity (psu) at ISMAR buoy. The gaps in the black line are missing observations.

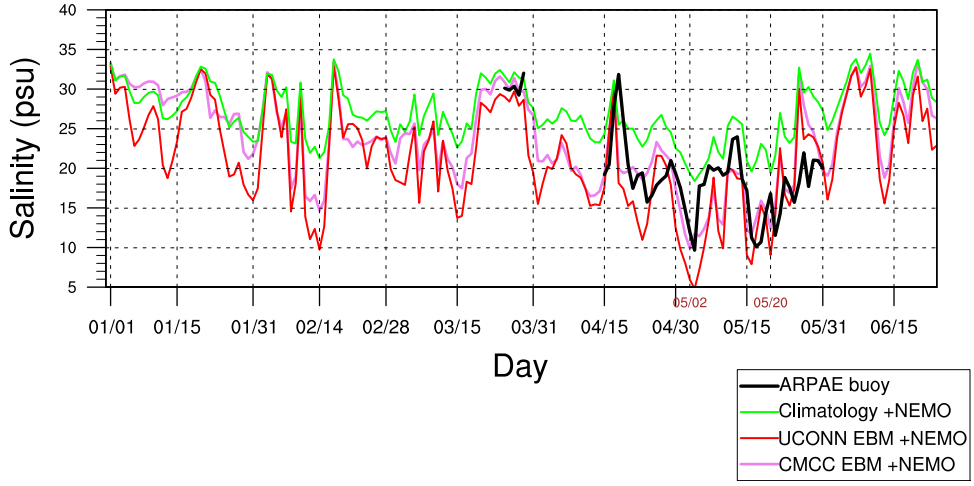


**Fig. 11.** Time series of observed and modelled salinity (psu) at ArpaE buoy. The gaps in the black line are missing observations.

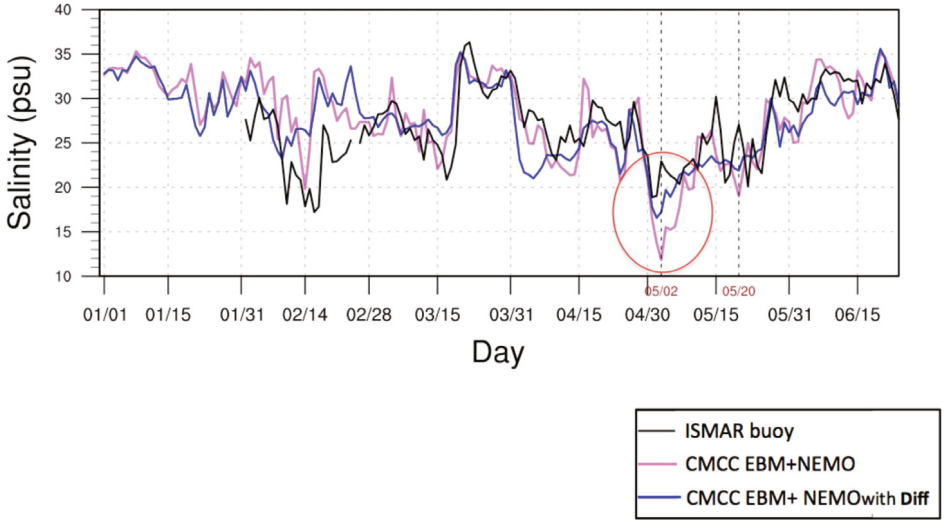


**Fig. 12.** Time series of observed and modelled salinity (psu) at ISMAR buoy by comparing the NEMO code with and without augmented vertical diffusivity at delta mouths.

In order to understand some of the discrepancies between the model and the observations shown in Fig. 10, we modified the vertical mixing parametrization near the river mouth. The development of river plumes is due to the outflowing river runoff and salinity and to a combination of wind forcing, tidal forcing, Coriolis effect and vertical mixing next to the river mouth (Kourafalou, 1999). In order to show the sensitivity of the Po plume to the vertical mixing in the ROFI area, we produced a specific analysis around May 2nd, when both EBMs failed to reproduce a correct value for the salinity in the plume with respect to the observed value (Fig. 10). The vertical mixing at the river mouth was increased for the CMCC-EBM case (an additional vertical eddy mixing coefficient is prescribed) and in Fig. 12 we show the new time series which better reproduces the salinity for May 2nd with respect to the observed value. The lesson learned is that if we want to reproduce properly the river plume dynamics, at least specific parametrizations of vertical mixing are required, especially during large runoff events.

## 7. Summary and conclusions

The aim of this study was the development of proper interfaces between mesoscale eddy-resolving models and estuaries in order to simulate the ROFI dynamics. Sun et al. (2017) have already shown the importance of using an Estuary Box Model (EBM) to estimate outflowing salinities. In this study we presented a new EBM and we compared it with Sun et al. (2017).

We have proposed three different approaches for representing the estuarine dynamics: the Knudsen relations model, the UCONN-NCAR EBM and our new model called CMCC EBM. The first two are a benchmark for representing the estuarine dynamics and we use them as the starting point of our investigation. The CMCC EBM aims at representing the estuarine processes in a different way than the UCONN-NCAR EBM because it is developed for coupling with an eddy resolving ocean numerical model which could resolve the subsurface flow input to the estuary. Furthermore, tidal volume flux contributes to the volume conservation equation and tidal mixing is parameterized in a different way to allow for partially mixed estuaries to be modelled.

We tested the coupling of the different EBMs with an eddy resolving regional ocean model covering the Adriatic Sea and for two different river dominated shelf areas: the highly stratified estuary of the Ofanto river and the partially mixed delta of the Po river.

The experiments prove that: (i) Knudsen's relation is a too simple approach, (ii) the CMCC EBM results are close to the UCONN-NCAR EBM for the Ofanto but differ for the Po where tides play a more significant role. The two EBMs are based on a different set of equations and one of the most important differences is the representation of the tidal effects in terms of both tidal pumping and tidal mixing processes. One of the strengths of the CMCC EBM is that it includes only 4 tunable parameters, less than in UCONN-NCAR, which is desirable as most estuaries are poorly monitored.

The coupled EBM and ocean model experiments show how the coastal dynamics are affected by the volume outflow $Q_{ul}^{ebm}$ and outflowing salinity $S_{ul}^{ebm}$ estimated by the EBMs. They prove that: (i) the CMCC EBM and UCONN-NCAR EBM coupled to a regional eddy-resolving model are capable of reconstructing river plumes and they both outperform the "climatological approach"; (ii) the CMCC EBM coupled system shows the lowest statistical errors compared to the observed salinity at two buoys located off the mouths of the Po. These findings encourage us to use the EBMs as main forcing submodels in shelf areas instead of the classical climatological imposition of an ad-hoc salinity value.

Overall we conclude that modelling the estuarine dynamics as a 2-layer exchange flow with tidally-averaged conservation equations is a relatively good representation of the exchange flow at the river mouth. The results of the EBMs could thus be used to appropriately force global/regional ocean models on a daily scale.

However, a weakness of all the EBMs discussed is the assumed steady estuarine dynamics. The reconstruction of the intrusion of the salt wedge in short temporal scales or the prediction of extreme events, e.g. the "blocking effect" in both directions due to storm surges or river flooding and the "Mascaret" occurring during the flood tide phase, requires a more sophisticated unsteady dynamics box model or the direct modeling of the river estuary. To further develop the estuarine box approach, the next step would be to consider the estuary length as a time-varying function of the river discharge and the tidal mixing. We plan to evaluate the role of the heat flux in the estuary water exchange by adding a temperature equation in the CMCC EBM and the wind forcing.

Finally, the near-mouth mixing processes as currently parameterized by the ocean eddy resolving model deserve a dedicated study in order to get the maximum benefit from the coupled EBM and ocean model system.

## Declaration of competing interest

The authors declare that they have no known competing financial interests or personal relationships that could have appeared to influence the work reported in this paper.

## CRediT authorship contribution statement

**Giorgia Verri:** Conceptualization, Methodology, Software, Validation, Investigation, Writing - original draft, Writing - review & editing, Formal analysis, Data curation, Resources. **Nadia Pinardi:** Conceptualization, Methodology, Writing - original draft, Writing - review & editing, Resources, Supervision. **Frank Bryan:** Methodology, Writing - review & editing, Resources. **Yu-heng Tseng:** Methodology, Writing - review & editing, Resources. **Giovanni Coppini:** Writing - review & editing, Funding acquisition, Resources, Project administration. **Emanuela Clementi:** Writing - review & editing.

## Acknowledgements

The authors are very grateful to Dr. Mariangela Ravaioli and Dr. Francesco Riminucci from the National Research Council of Italy-Institute of Marine Sciences (CNR-ISMAR) and to Dr. Andrea Valentini from the Regional Agency for the environmental protection of Emilia Romagna Region (ArpaE) for providing the observational datasets of the buoys used in this study. CMCC research activities were supported by the EU Copernicus Marine Environment Monitoring Service projects of the Mediterranean Sea Monitoring and Forecasting (n.74-CMEMS-MFC-MED-N) and of the Black Sea Monitoring and Forecasting (n.72-CMEMS-MFC-BS-N), and marginally by the Apulia Region funded project SAGACE (Innonetwork n. M7X3HL2). Frank Bryan's participation in this study was supported by the National Center for Atmospheric Research, NCAR, which is a major facility sponsored by the US National Science Foundation under Cooperative Agreement No. 1852977. We would also like to thank Dr. Joe Tribbia of the Division of Climate and Global Dynamics at the NCAR in Boulder CO, for his valuable suggestions.

## Appendix A. Governing equations of the CMCC EBM

We deduce (7) starting from the incompressible continuity equation:

$$\nabla \cdot \vec{u} = 0 \tag{12}$$

Considering the volume integral over the estuary box we obtain:

$$\int\int\int_V \nabla \cdot \vec{u} dV = \int\int_S \vec{u} \cdot \hat{n} dS = 0 \tag{13}$$

where $\hat{n}$ is unit normal field pointing outward the surface $S$ bounding the estuary volume. In the box model, the sections at the estuary mouth and head are the only open lateral boundaries, as shown in Fig. A.1. We assume the estuarine box to have equal layer thicknesses between

the surface and $H$ depth. Furthermore we assume that the river inflow occurs only in the upper layer, at the head section. Thus (13) becomes:

$$\int_{H/2}^{H}\int_{dy}\vec{u}_{ul}^{ebm}\cdot\hat{n}\,dz\,dy-\int_{H/2}^{H}\int_{dy}\vec{u}_{river}\cdot\hat{n}\,dz\,dy\;+$$
$$-\int_{0}^{H/2}\int_{dy}\vec{u}_{ll}^{ocean}\cdot\hat{n}\,dz\,dy-\int_{0}^{H}\int_{dy}\vec{u}_{baro}^{ocean}\cdot\hat{n}\,dz\,dy=0$$
$$Q_{ul}^{ebm}-Q_{river}-Q_{ll}^{ocean}-Q_{tide_f}^{ocean}=0 \tag{14}$$

where the last term on the LHS of the two equations is the barotropic ocean water inflow driven by tides. We write the volume fluxes in (14) as follows:

$$Q_{ul}^{ebm}=u_{ul}^{ebm}\frac{H}{2}L_y \tag{15}$$
$$Q_{ll}^{ocean}=u_{ll}^{ocean}\frac{H}{2}L_y \tag{16}$$
$$Q_{tide_f}^{ocean}=HL_yu_{tide_f} \tag{17}$$
$$Q_{river}=u_{river}\frac{H}{2}L_y \tag{18}$$

where it is assumed that $\vec{u}_{baro}^{ocean}\cdot\hat{n}=u_{tide_f}$ is the velocity of the flood tide entering the estuary, weighted over the estuary depth. The $u_{tide_f}$ is computed from the hourly outputs of the Oregon State University Tidal Prediction Software (OTPS, Egbert and Erofeeva, 2002), considered as flood tide values if landward oriented and daily averaged. The outgoing tidal velocity during the ebb tide is embedded into the unknown estuarine water outflow $Q_{ul}^{ebm}$ thus it does not appear explicitly in the equations. Eq. (14) is the final volume conservation equation for the CMCC EBM, together with the definitions (15), (16), (17), and (18).

The salinity equation, considered at steady state is written:

$$\nabla\cdot(\vec{u}S)=K_{S_x}\frac{\partial^2S}{\partial x^2}+K_{S_y}\frac{\partial^2S}{\partial y^2}+K_{S_z}\frac{\partial^2S}{\partial z^2} \tag{19}$$

where $(K_{S_x},K_{S_y})$ and $K_{S_z}$ are the horizontal and vertical diffusivity coefficients respectively. The volume integral of (19) reads:

$$\int\int\int_V\nabla\cdot(\vec{u}S)dV=\int\int\int_V K_{S_x}\frac{\partial^2S}{\partial x^2}dV \tag{20}$$

The across-estuary and vertical diffusive salt flux does not appear explicitly in the volume averaged salinity equation as a result of the insulated boundaries at the surface, bottom and side walls. We assume that the along-estuary diffusion of salinity is driven by the barotropic tidal inflow. Thus the volume integral of (20) reduces to:

$$\int\int_\Omega\vec{u}S\cdot\hat{n}d\Omega=L_yH\int_{x=0}^{x=-L_x}K_{S_x}\frac{\partial^2\overline{S}}{\partial x^2}dx \tag{21}$$
$$=L_yHK_{S_x}\left[\frac{\partial\overline{S}}{\partial x}\right]_{x=0}^{x=-L_x} \tag{22}$$
$$\sim L_yHK_{S_x}\frac{\overline{S}(x=-L_x)-\overline{S}(x=0)}{-L_x}$$
$$=K_{S_x}H\frac{L_y}{L_x}\overline{S}_{ocean} \tag{23}$$

where $-L_x$ is the estuary head position, where salinity is zero, $\overline{S}(x=0)=\overline{S}_{ocean}$ is the vertically integrated salinity at the estuary mouth. For the horizontal diffusivity coefficient we use (Banas et al., 2004), $K_{S_x}=0.035\,L_y\,u_{tide_f}$.

By considering the salinity fluxes at the estuary head and mouth cross sections, (20) can now be rewritten as follows:

$$\int_{H/2}^{H}\int_{dy}u_{ul}^{ebm}S_{ul}^{ebm}\cdot\hat{n}dzdy\Big|_{x=0}-\int_{0}^{H/2}\int_{dy}\vec{u}_{ll}^{ocean}S_{ll}^{ocean}\cdot\hat{n}dzdy\Big|_{x=0}+ \tag{24}$$
$$-\int_{0}^{H}\int_{dy}\overline{S}_{ocean}\vec{u}_{baro}^{ocean}\cdot\hat{n}dzdy\Big|_{x=0}=K_{S_x}H\frac{L_y}{L_x}\overline{S}_{ocean}$$

with the following definitions:

$$\int_{H/2}^{H}\int_{dy}u_{ul}^{ebm}S_{ul}^{ebm}\cdot\hat{n}dzdy\Big|_{x=0}=Q_{ul}^{ebm}S_{ul}^{ebm} \tag{25}$$

$$\int_{0}^{H/2}\int_{dy}\vec{u}_{ll}^{ocean}S_{ll}^{ocean}\cdot\hat{n}dzdy\Big|_{x=0}=Q_{ll}^{ocean}S_{ll}^{ocean} \tag{26}$$

$$\int_{0}^{H}\int_{dy}\overline{S}_{ocean}\vec{u}_{baro}^{ocean}\cdot\hat{n}dzdy\Big|_{x=0}=HL_yu_{tide_f}\overline{S}_{ocean} \tag{27}$$

where the river salinity flux at the estuary head is assumed to be zero and the other symbols have been previously defined. By replacing (25), (26), (27) in (24), we finally obtain (8).

## Appendix B. Formulation of the surface salinity boundary condition

The continuity and the salinity equations used in the regional eddy resolving ocean model of this paper are:

$$\nabla\cdot\vec{u}_h+\frac{\partial w}{\partial z}=0 \tag{28}$$

$$\frac{\partial S}{\partial t}+\nabla_h\cdot(\vec{u}_hS)+\frac{\partial wS}{\partial z}=\nabla_h\cdot\vec{F}_S^H+\frac{\partial(F_S^V)}{\partial z} \tag{29}$$

where $\vec{F}_S=(\vec{F}_S^H,F_S^V)$ is the (negative of) diffusive salt flux with the horizontal components, $\vec{F}_S^H=(K_h\frac{\partial S}{\partial x},K_h\frac{\partial S}{\partial y})$ and the vertical component $F_S^V=K_v\frac{\partial S}{\partial z}$. The surface boundary conditions at $z=\eta$ for Eqs. (28) and (29) read as follows (Beron-Vera et al., 1999; Tseng et al., 2016):

$$w\Big|_{z=\eta}-\frac{\partial\eta}{\partial t}-\vec{u}_h\Big|_{z=\eta}\cdot\nabla_h\eta=-q_w \tag{30}$$

$$S(\eta)(w\Big|_{z=\eta}-\frac{\partial\eta}{\partial t}-\vec{u}_h\Big|_{z=\eta}\cdot\nabla_h\eta)-F_S^V+\vec{F}_S^H\cdot\nabla\eta=-q_wS_w+Q_s \tag{31}$$

where

$$q_w=(P+Q_{ul}^{ebm}/A-E) \tag{32}$$

is the water volume addition at the air–sea interface considering the volume flux $Q_{ul}^{ebm}$ from the EBMs to be inserted at the surface (A is the horizontal area of the river mouth), $S(\eta)$ is the ocean model surface salinity, $S_w$ is the salt associated with the water specifically entering or exiting the sea by advection and $Q_S$ is the salt entering or exiting by turbulent processes. Note that (30) and (31) admit both water and salt crossing the surface, thus the sea surface is not a material surface with respect to salt and water. Assuming that the horizontal diffusive salt flux $\vec{F}_S^H$ is negligible with respect to the vertical $F_S^V$ and using (30) into (31), we rewrite the boundary condition for the salinity at the surface, i.e.:

$$F_S^V=K_v\frac{dS}{dz}\Big|_{z=\eta}=-q_wS(\eta)+q_wS_w-Q_s \tag{33}$$

We assume:

$$q_wS_w=(P-E)S_{EP}+Q_{ul}^{ebm}/A\;S_{ul}^{ebm} \tag{34}$$

and

$$Q_s=-Q_{ul}^{ebm}/A\;S(\eta) \tag{35}$$

In (34) we consider the salinity of evaporation and precipitation to be zero, i.e. $S_{EP}=0$ while the turbulent salinity flux (35) considers the dilution due to the runoff term. At the surface of a river mouth, salinity is a mixture of upstream river freshwaters and the marine waters entering the estuary, as computed by the box models of this paper. The surface salinity values at the river mouth are then different from the values in areas just offshore the river mouth.

In a lateral open boundary condition framework, rivers have a net dilution effect because the entering surface waters have lower salinities than in the offshore. In a closed lateral boundary condition framework, using the surface salt boundary condition (33), rivers dilution effects are parameterized with (35).

Using (34) and (35) in (33) we obtain the used salinity boundary condition:

$$K_v\frac{\partial S}{\partial z}\Big|_{z=\eta}=(E-P)S(\eta)+Q_{ul}^{ebm}/A\;S_{ul}^{ebm} \tag{36}$$

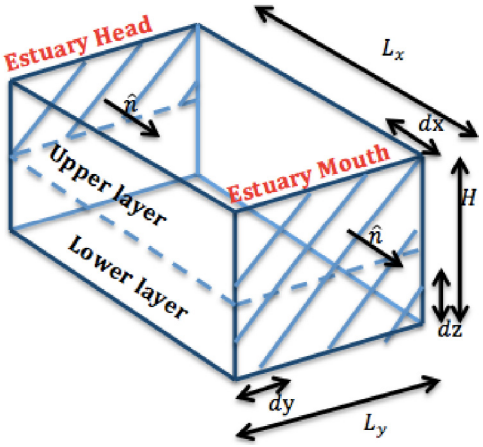


**Fig. A.1.** Schematic representation of the estuary box: 2-layer rectangular box with constant width $L_y$, length $L_x$, and depth $H$. Shaded cross sections are the open boundaries. The mouth of the estuary box is defined at the origin of the $x$-axis with its positive toward the ocean. The vertical $z$-axis is defined positive upward with the origin at the bottom of the estuary mouth.

The salt conserving formulation of (33) in the river closed lateral boundary condition context, i.e. the natural boundary condition approach, considers the subtraction of the salt entering at the surface in the subsurface (see Tseng et al., 2016).

## References


Banas, N.S., Hickey, B.M., MacCready, P., Newton, J.A., 2004. Dynamics of Willapa Bay, Washington: A highly unsteady, partially mixed estuary. J. Phys. Oceanogr. 34 (11), 2413–2427.

Beron-Vera, F., Ochoa, J., Ripa, P., 1999. A note on boundary conditions for salt and freshwater balances. Ocean Model. 1, 111–118.

Chao, S.Y., 1987. Wind driven motion near inner shelf fronts. J. Geophys. Res.: Oceans 92 (C4), 3849–3860.

Chapman, D.C., Beardsley, R.C., 1989. On the origin of shelf water in the Middle Atlantic. J. Phys. Oceanogr. 19 (3), 384–391.

Chen, S., Sanford, L., 2009. Axial wind effects on stratification and longitudinal salt transport in an idealized partially mixed estuary. J. Phys. Oceanogr. 39, 1905–1920.

Coles, V.J., Brooks, M.T., Hopkins, J., Stukel, M.R., Yager, P.L., Hood, R.R., 2013. The pathways and properties of the Amazon River Plume in the tropical North Atlantic Ocean. J. Geophys. Res. 118 (12), 6894–6913.

Egbert, G.D., Erofeeva, S.Y., 2002. Efficient inverse modeling of barotropic ocean tides. J. Atmos. Ocean. Technol. 19 (2), 183–204.

Fischer, H., List, E., Koh, R., Imberger, J., Brooks, N., 1979. Mixing in Inland and Coastal Waters. Academic Press, New York.

Garvine, R.W., 1999. Penetration of buoyant coastal discharge onto the continental shelf: A numerical model experiment. J. Phys. Oceanogr. 29 (8), 1892–1909.

Garvine, R.W., Whitney, M.M., 2006. An estuarine box model of freshwater delivery to the coastal ocean for use in climate models. J. Mar. Res. 64 (2), 173–194.

Geyer, W.R., Smith, J.D., 1987. Shear instability in a highly stratified estuary. J. Phys. Oceanogr. 17 (10), 1668–1679.

Guarnieri, A., Pinardi, N., Oddo, P., Bortoluzzi, G., Ravaioli, M., 2013. Impact of tides in a baroclinic circulation model of the Adriatic Sea. J. Geophys. Res. Oceans 118 (1), 166–183.

Hordoir, R., Polcher, J., Brun-Cottan, J., Madec, G., 2008. Towards a parametrization of river discharges into ocean general circulation models: a closure through energy conservation. Clim. Dyn. 31 (7-8), 891–908.

Jirka, G.H., Adams, E.E., Stolzenbach, K.D., 1981. Buoyant surface jets. J. Hydraul. Div. Proc. ASCE 107 (HY11), 1467–1487.

Knudsen, M., 1900. Ein hydrographischer lehrsatz. Ann. Hydrogr. Mar. Meteorol..

Kourafalou, V., 1999. Process studies on the Po River plume, North Adriatic Sea. J. Geophys. Res. 104 (C2), 29963–29985.

Kourafalou, V., Oey, L., Wang, J., Lee, T., 1996. The fate of river discharge on the continental shelf. 1.Modeling the river plume and the inner-shelf coastal current. J. Geophys. Res. 101 (C2), 3415–3434.

Ludwig, W., Dumont, E., Meybeck, M., Heussner, S., 2009. River discharges of water and nutrients to the Mediterranean and Black Sea: major drivers for ecosystem changes during past and future decades. Prog. Oceanogr. 80, 199–217.

MacCready, P., Banas, N., Hickey, B., Dever, E., Liu, Y., 2009. A model study of tide and wind-induced mixing in the Columbia River Estuary and plume. Cont. Shelf Res. 29 (1), 278–291.

MacCready, P., Geyer, W.R., 2010. Advances in Estuarine Physics. Annu. Rev. Mar. Sci. 2 (1), 35–58.

Madec, G., 2008. NEMO Ocean Engine. Note du Pole de Modelisation, Vol. 27. Institut Pierre-Simon Laplace (IPSL), France, pp. 1288–1619.

Oddo, P., Adani, M., Pinardi, N., Fratianni, C., Tonani, M., Pettenuzzo, D., 2009. A nested Atlantic-Mediterranean Sea general circulation model for operational forecasting. Ocean Sci..

Oddo, P., Pinardi, N., Zavatarelli, M., 2005. A numerical study of the interannual variability of the Adriatic Sea (2000-2002). Sci. Total Environ. 353 (1-3), 39–56.

Provini, A., Crosa, G., Marchetti, R., 1992. Nutrient export from the Po and Adige river basins over the last 20 years. Mar. Coast. 291–313.

Rahmstorf, S., 1995. Bifurcations of the Atlantic thermohaline circulation in response to changes in the hydrological cycle. Nature 378, 145–149.

Raicich, F., 1996. Note on the flow rates of the Adriatic rivers. In: CNR. Istituto Talassografico di Trieste Tech. Rep. RF 02/94, Available from CNR Istituto Talassografico, Trieste Italy, p. 8.

Ravaioli, M., Bergami, C., Riminucci, F., Langone, L., Cardin, V., Di Sarra, A., Aracri, A., Bastianini, M., Bensi, M., Bergamasco, A., Bommarito, C., Borghini, M., Bortoluzzi, G., Bozzano, R., Cantoni, C., Chiggiato, J., Crisafi, E., D'Adamo, R., Durante, S., Fanara, C., Grilli, F., Lipizer, M., Marini, M., Miserocchi, S., Paschini, E., Penna, P., Pensieri, S., Pugnetti, A., Raicich, F., Schroeder, K., Siena, G., Specchiulli, A., Stanghellini, G., Vetrano, A., Crise, A., 2016. The RITMARE Italian Fixed-point Observatory Network (IFON) for marine environmental monitoring: a case study. J. Oper. Oceanogr. 9 (S1), 202–214.

Schiller, R., Kourafalou, V., 2010. Modeling river plume dynamics with the HYbrid Coordinate Ocean Model. Ocean Model. 33, 101–117.

Schroeder, W., Wiseman Jr., W., 1986. Low-frequency shelf-estuarine exchange processes inMobile Bay and other estuarine systems on the northern Gulf of Mexico. In: Wolfe, D.A. (Ed.), Estuarine Variability. Academic Press, NY, pp. 355–366.

Scully, M., Friedrichs, C., Brubaker, J., 2005. Control of estuarine stratification and mixing by wind-induced straining of the estuarine density field. Estuaries 28, 321–326.

Simpson, J., Bos, W., Shirmer, F., Souza, A., Rippeth, T., Jones, S., Hydes, D., 1993. Periodic stratification in the Rhine ROFI in the North Sea. Oceanol. Acta 16 (1), 23–32.

Simpson, J., Brown, J., Matthews, J., Allen, G., 1990. Tidal straining, density currents, and stirring in the control of estuarine stratification. Estuaries 13, 125–132.

Skliris, N., Sofianos, S., Lascaratos, A., 2007. Hydrological changes in the Mediterranean Sea in relation to changes in the freshwater budget: a numerical modelling study. J. Mar. Syst. 65, 400–416.

Stommel, H., Farmer, H., 1995. On the Nature of Estuarine circulation. In: Hogg, N.G., Rui Xin Huang (Eds.), Collected Works of Stommel H. M.. American Meteorological Society III, pp. 526–568.

Sun, Q., Whitney, M.M., Bryan, F.O., Tseng, Y.H., 2017. A box model for representing estuarine physical processes in Earth system models. Ocean Model. 112, 139–153.

Sun, Q., Whitney, M.M., Bryan, F.O., Tseng, Y.H., 2019. Assessing the skill of the improved treatment of riverine freshwater in the Community Earth System Model (CESM) relative to a new salinity climatology. J. Adv. Mod. Earth Sys. 11, 1189–1206. http://dx.doi.org/10.1029/2018MS001349.

Tseng, Y.-H., Bryan, F.O., Whitney, M.M., 2016. Impacts of the representation of riverine freshwater input in the Community Earth System Model. Ocean Model. 105, 71–86.

Verri, G., Pinardi, N., Gochis, D., Tribbia, J., Navarra, A., Coppini, G., Vukicevic, T., 2017. A meteo-hydrological modelling system for the reconstruction of river runoff: the case of the ofanto river catchment. Nat. Hazards Earth Syst. Sci. 17 (10), 1741–1761.

Verri, G., Pinardi, N., Oddo, P., Ciliberti, S., Coppini, G., 2018. River runoff influences on the Central Mediterranean Overturning Circulation. Clim. Dynam. 50 (5-6), 1675–1703.

Yankovsky, A., Chapman, D., 1997. A simple theory for the fate of buoyant coastal discharges. J. Phys. Oceanogr. 27, 1386–1401.